



## Domain Interactions in the Fab Fragment: A Comparative Evaluation of the Single-chain Fv and Fab Format Engineered with Variable Domains of Different Stability

Daniela Röthlisberger, Annemarie Honegger and Andreas Plückthun\*

Biochemisches Institut  
Universität Zürich  
Winterthurerstrasse 190  
CH-8057 Zürich, Switzerland

Recombinant antibody fragments, most notably Fab and scFv, have become important tools in research, diagnostics and therapy. Since different recombinant antibody formats exist, it is crucial to understand the difference in their respective biophysical properties. We assessed the potential stability benefits of changing the scFv into the Fab format, the influence of the variable domains on the stability of the Fab fragment, and the influence of the interchain disulfide bond in the Fab fragment. To analyze domain interactions, the Fab fragment was broken down into its individual domains, several two-domain assemblies and one three-domain assembly. The equilibrium denaturation properties of these constructs were then compared to those of the Fab fragment. It was found that mutual stabilization occurred across the V<sub>H</sub>/V<sub>L</sub> and the C<sub>H1</sub>/C<sub>L</sub> interface, whereas the direct interaction between the V<sub>L</sub> and the C<sub>L</sub> domain had no influence on the stability of either domain. This observation can be explained by the different interfaces used for interaction. In contrast, the whole C<sub>H1</sub>C<sub>L</sub> and V<sub>H</sub>V<sub>L</sub> unit showed significant mutual stabilization, indicating a high degree of cooperation between the V<sub>H</sub>/V<sub>L</sub> and C<sub>H1</sub>/C<sub>L</sub> interface. The interchain disulfide bond in the Fab fragment plays an essential role in this stabilization. In addition to the effects of domain association on the thermodynamic (equilibrium) stability, Fab fragments differ from scFv fragments of similar equilibrium stability by having a very slow unfolding rate. This kinetic stabilization may increase significantly the resistance of Fab fragments against short time exposure to adverse conditions.

© 2005 Elsevier Ltd. All rights reserved.

\*Corresponding author

**Keywords:** antibody fragment; domain interaction; mutual stabilization

### Introduction

Recombinant antibodies have become widely used reagents in research, diagnostics and therapy.<sup>1–8</sup> They can now be made in fully human form against essentially any target, by a variety of technologies.<sup>9–10</sup> Some advantages of whole antibodies include a long half-life in the

blood circulation as well as the ability to activate complement and to engage Fc receptor-mediated effector functions.<sup>11–13</sup> Although the presence of the Fc is desirable for many therapeutic applications, other therapeutic, diagnostic and technical applications do not rely on the natural effector functions of antibodies. Consequently, antigen-binding fragments of antibodies smaller than

Abbreviations used: V<sub>H</sub>, V<sub>L</sub>, variable domains of the antibody heavy and light chain; V<sub>H</sub><sup>W</sup>, V<sub>H</sub> with weak stability; V<sub>H</sub><sup>M</sup>, V<sub>H</sub> with medium stability; V<sub>H</sub><sup>S</sup>, V<sub>H</sub> with strong stability; V<sub>L</sub><sup>W</sup>, V<sub>L</sub> with weak stability; V<sub>L</sub><sup>S</sup>, V<sub>L</sub> with strong stability; C<sub>L</sub>, constant domains of the antibody light chain; C<sub>H1</sub>, first constant domain of the antibody heavy chain; C<sub>H1</sub>C<sub>L</sub>, fragment, two-domain assembly consisting of C<sub>H1</sub> and C<sub>L</sub> domains; C<sub>H1</sub>C<sub>L</sub><sup>frag</sup>, fragment, C<sub>H1</sub>C<sub>L</sub> fragment with interchain disulfide bond; Fab fragment, antigen-binding fragment consisting of V<sub>H</sub>, C<sub>H1</sub>, V<sub>L</sub> and C<sub>L</sub>; Fab<sup>85</sup>, fragment, Fab fragment with an interchain disulfide bond; Fd fragment, antibody heavy chain fragment consisting of V<sub>H</sub> and C<sub>H1</sub>; Fc fragment, dimer of the region of the heavy chain C-terminal to the hinge; scFv fragment, single-chain Fv fragment; scFv-C<sub>L</sub>, fragment, scFv fragment with the C<sub>L</sub> domain covalently linked to V<sub>L</sub>; IgG, immunoglobulin G; GdnHCl, guanidine hydrochloride.

E-mail address of the corresponding author: plueckthun@bioi.unizh.ch

immunoglobulin G (IgG) are now being considered for many applications. Such recombinant antibody fragments offer several advantages. They can be produced in bacteria in functional form,<sup>11</sup> greatly simplifying the access to these molecules. Their smaller size allows improved tissue penetration for therapeutic applications, such as cancer therapy.<sup>11</sup> Moreover, a number of strategies exist to produce these fragments in multivalent form (either unispecific or multi-specific),<sup>15,16</sup> and this ultimately confers increased control over size and avidity. Finally, a wide variety of peptidic tags or protein domains can be used for detection and controlled immobilization of recombinant antibody fragments. Because of these many options, it is essential to understand the biophysical properties of the various antibody formats and, in particular, the interaction of different domains in the antibody fragment. Therefore, the effect of the constant domains on the stability of variable domains with different stabilities was investigated in the context of the antigen-binding Fab fragment consisting of V<sub>H</sub>, C<sub>H</sub>1, V<sub>L</sub> and C<sub>L</sub>.

The IgG molecule is a modular protein, consisting of two identical heavy chains, folded into four domains (V<sub>H</sub>, C<sub>H</sub>1, C<sub>H</sub>2 and C<sub>H</sub>3), and two identical light chains, folded into two domains (V<sub>L</sub> and C<sub>L</sub>). The four chains associate to form three structural units. Two units are Fab fragments consisting each of V<sub>L</sub>, C<sub>L</sub>, V<sub>H</sub> and C<sub>H</sub>1 domains. The third unit is the dimer of the region of the heavy chain C-terminal to the hinge (Fc fragment) consisting of two C<sub>H</sub>2 and two C<sub>H</sub>3 domains. Fab and Fc fragments are connected loosely by a hinge region in the heavy chain and are not believed to interact structurally with each other.<sup>17,18</sup> The smallest antibody entity retaining the antigen specificity of its parental antibody consists of a heterodimer of the V<sub>H</sub> and V<sub>L</sub> variable domains, the so-called Fv fragment.<sup>19</sup> In most Fv fragments, the dissociation constant between the V<sub>H</sub> and V<sub>L</sub> domains, which ranges from  $10^{-5}$  M to  $10^{-8}$  M,<sup>20-24</sup> is not sufficient to keep the domains associated at low concentrations of protein or under mildly destabilizing conditions. To avoid this problem in recombinantly produced constructs, the variable domains are usually connected by a genetically encoded flexible peptide linker, either in the orientation V<sub>H</sub>-linker-V<sub>L</sub> or V<sub>L</sub>-linker-V<sub>H</sub>, resulting in a single-chain Fv (scFv) fragment.<sup>21,25-27</sup> The scFv fragment has become the most popular antibody format, because of its small size (30 kDa), the presence of only one polypeptide chain, and the relative ease with which it is produced in bacteria. Moreover, since it is composed of a single polypeptide chain, fusion proteins can be constructed easily.

The larger Fab fragments (50 kDa), which include the C<sub>L</sub> domain and the first of the C<sub>H</sub> domains, are preferred by a number of researchers because they are perceived to be more stable than scFv fragments, even though there is little published

evidence supporting this. In one study, a Fab fragment containing variable domains of marginal stability appeared to be more stable than the corresponding Fv fragments, but the scFv was not investigated in this study.<sup>28</sup> The current literature gives little indication of whether this holds true for all scFv/Fab fragment pairs, or if at higher variable domain stability the intrinsic stability of the constant domains becomes limiting. Immunoglobulin variable domains differ widely in their intrinsic stabilities. This has been demonstrated for a series of V<sub>L</sub> and V<sub>H</sub> domains representing the consensus sequences of the major human germline families.<sup>29</sup> The stability of weak variable domains can often be improved dramatically by the introduction of a limited number of stabilizing mutations,<sup>30,31</sup> or by directed evolution selecting for improved stability.<sup>32-34</sup> The questions remain to what extent the stability of a Fab fragment can be improved by increasing the stability of the constituent variable domains and if the stabilities of the constant domains become limiting at some point. Hence, we performed this study in the context of variable domains that differ significantly in their intrinsic stability.

Early studies of the stability of a particular Fab fragment,<sup>35</sup> compared to that of the light chain alone,<sup>36</sup> showed a significant stabilization of the light chain through interactions with the heavy chain. Within the context of a disulfide-linked Fab fragment, the V<sub>H</sub>V<sub>L</sub> heterodimer and the C<sub>H</sub>C<sub>L</sub> heterodimer were found to behave as two distinct folding units. The C<sub>H</sub>C<sub>L</sub> heterodimer was found to be significantly more stable than the V<sub>H</sub>V<sub>L</sub> heterodimer for the particular antibody under study. In addition, its denaturation was found to be extremely slow, requiring weeks to months to reach equilibrium.<sup>36</sup>

In naturally occurring antibodies, heavy and light chains of the Fab fragment are usually connected by a disulfide bond that is structurally located at the "bottom" of the constant domains. Although the sequence position of the participating cysteine residues is not conserved between different immunoglobulin types, the spatial location is indeed very similar (described in detail in Discussion). We were interested in investigating the contribution of this interchain disulfide bond to stability in the context of variable domains with very different stabilities.

From a series of closely related variable domains of different stability, derived from the antibodies ABPC48 and 4D5, previously analyzed in the context of the scFv fragment,<sup>37</sup> we constructed Fab fragments with and without a disulfide bond connecting the two chains. Urea and/or guanidine hydrochloride (GdnHCl) unfolding curves were determined for the isolated domains as well as for the different combinations of variable domains in the scFv format (V<sub>H</sub>-linker-V<sub>L</sub>), in the unlinked Fab format and in the disulfide-linked Fab format (Fab<sup>SS</sup>). In addition, the unfolding curves of the isolated light chain (V<sub>L</sub>C<sub>L</sub>), the disulfide-linked

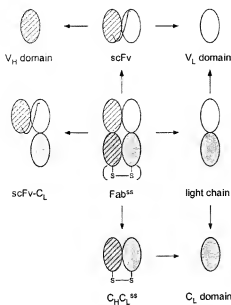


**Figure 1.** Dissection of the Fab fragment. All the antibody domain assemblies that were investigated are depicted. The investigation of the isolated  $C_{H1}C_L$  domain and the Fd fragment ( $V_H$  and  $C_H1$ ) was not possible due to degradation and aggregation, respectively. Fab fragments with and without the C-terminal interchain disulfide bond were studied. This was not possible for the  $C_H1C_L$  assembly. Because of the weak interaction across the interface, only the disulfide-bonded version resulted in a homogenous protein preparation. With these different assemblies, it was possible to untangle the contributions of the intrinsic domain stability and interface stabilization to the overall stability of the Fab fragment. The denaturation curves of two isolated  $V_L$  domains with low ( $V_L^w$ ) and with high ( $V_L^s$ ) stability, and three isolated  $V_H$  domains with very low ( $V_H^w$ ), medium ( $V_H^m$ ) and high ( $V_H^s$ ) intrinsic stability were determined.

## Results

### Constructs analyzed

The antibody fragments used in this study were derived from the murine myeloma protein ABPC48,<sup>36</sup> a levan (poly- $\beta$ -2, 6-D-fructose) binding antibody,<sup>37</sup> and the humanized monoclonal antibody 4D5, which binds HER2.<sup>39</sup> To assess the domain interaction and mutual stabilization, variable domains with different intrinsic stability were combined. The stable  $V_L$  domain, named  $V_L^s$  (superscript s for strong), is derived from the antibody 4D5, while the weak  $V_L$  domain, named  $V_L^w$  (superscript w for weak), comes from ABPC48. For the  $V_H$  domains, three different stability mutants were used (Table 1). The  $V_H$  domain with the lowest stability, named  $V_H^w$ , is derived from the wild-type ABPC48 sequence. It does not have a disulfide bond, as the conserved cysteine H92 is naturally replaced by a tyrosine residue,<sup>40</sup> and the unpaired cysteine H22 has been replaced by alanine<sup>41</sup> to prevent unwanted oxidation (numbering according to Kabat<sup>42</sup>). As the unmodified wild-type  $V_H$  domain would be too unstable for characterization in the absence of the  $V_L$  domain, the stabilizing mutation LysH66Arg was introduced to give  $V_H^m$ .<sup>37</sup> The mutant of intermediate stability, named  $V_H^m$  (superscript m for medium), has two additional stabilizing mutations, AsnH52Ser and TyrH92Val. In the most stable  $V_H$  domain,  $V_H^s$ , the intradomain disulfide bond is restored in the context of the stabilizing mutations LysH66Arg and AsnH52Ser. The murine  $\kappa$  light chain ( $C_L$ ) sequence of the constructs analyzed in this study corresponds to the wild-type ABPC48 sequence. Since the murine IgA  $C_{H1}$  domain of wild-type ABPC48 does not form a disulfide bond with the C-terminal cysteine residue in the  $C_L$  domain, it was replaced by a murine IgG1  $C_{H1}$  domain. Constructs with the C-terminal interchain disulfide bond between the  $C_L$  and  $C_{H1}$  domain are denoted with the superscript SS. In the non-disulfide-linked constructs, the C-terminal cysteine residues were deleted in both the  $C_L$  and the  $C_{H1}$  domain.

### Protein expression and purification

The different Fab fragments, with and without the intermolecular disulfide bond (denoted  $Fab^{SS}$  and Fab fragment) and the scFv  $V_H^sV_L^s$  and  $V_H^sV_L^w$  fragments were expressed in soluble, native form in the periplasm of *Escherichia coli* and purified under

$C_{H1}C_L$  heterodimer ( $C_H1C_L^{SS}$ ) and an scFv- $C_L$  construct were analyzed (Figure 1). By this approach, we obtained global information on the relative stability of Fab fragments and scFv fragments as well as the mutual interface interaction of their constituent domains, and we could differentiate between the situation in molecules with very stable variable domains and those with very unstable ones.

**Table 1.** Overview of  $V_H$  domains used

Abbreviation	H22	H52	H66	H92	Intradomain disulfide bond
Wild-type	Cys	Asn	Lys	Tyr	No
$V_H^w$	Ala	Asn	Arg	Tyr	No
$V_H^m$	Ala	Ser	Arg	Val	No
$V_H^s$	Cys	Ser	Arg	Cys	Yes

non-denaturing conditions. The same procedure was used for the isolated  $V_L$  and  $C_L$  domain, the light chain and the disulfide-linked heterodimer of the constant domains ( $C_HC_S^{SS}$ ). While the unlinked  $C_HC_L$  heterodimer was expressed with reasonable yields under those conditions, dissociation during purification led to precipitation and loss of the  $C_H$  domain. The isolated  $V_H$  domains and the scFv  $V_H^W V_L^L$  fragment, containing the weak  $V_H^W$  domain lacking the intradomain disulfide bond, had to be expressed as inclusion bodies and refolded by fast dilution. Two constructs could not be studied: The isolated  $C_H1$  domain could not be expressed in significant amounts, neither by periplasmic expression nor as inclusion bodies in the cytoplasm of *E. coli*, probably due to the rapid degradation of the polypeptide chain. The denaturation curves of the antibody heavy chain fragment consisting of  $V_H$  and  $C_H1$  (Fd fragment) of the heavy chain could not be analyzed, presumably due to aggregation or multimerization in the transition region. Gel-filtration analysis confirmed that all purified fragments under investigation had the expected molecular mass and did not form oligomers under the conditions of the analysis (data not shown). The presence of the disulfide bond linking the heavy chain and the light chain in the Fab<sup>SS</sup> and  $C_HC_S^{SS}$  constructs was confirmed by SDS-PAGE under reducing and non-reducing conditions (data not shown).

### Equilibrium unfolding curves

Denaturant-induced equilibrium unfolding was followed by fluorescence spectroscopy, using an excitation wavelength of 280 nm (which excites both tyrosine and tryptophan residues) and measuring the emission spectrum between 320 nm and 365 nm. Given the complexity of the fluorescence changes upon unfolding of these multi-domain constructs, it is difficult to find a representation that allows the direct comparison of the unfolding behavior between different constructs. Fluorescence intensity data for antibody-derived constructs are often noisy due to the strong aggregation propensity of some unfolding intermediates, leading to light-scattering or errors in the protein concentration. In addition, some unfolding transitions lead to an increase of the quantum yield (unquenching of the core tryptophan residues, which are located next to a disulfide bond), while others lead to a decrease (e.g., exposure of the  $V_H/V_L$  interface tryptophan residues). In contrast, the emission maximum depends solely on the environment of the tryptophan residues detected. Fully solvent-exposed tryptophan residues show an emission maximum at 350 nm, which corresponds to pure tryptophan in aqueous solution,<sup>43</sup> while the hydrophobic interior of proteins causes a blue shift of the emission maximum. We therefore plot the shift in the wavelength of the fluorescence emission maximum as a function of denaturant concentration. This signal shows a monotonic increase

across all unfolding events, as disruption of interfaces and denaturation of domains leads to an increased solvent exposure of tryptophan residues and therefore causes a red-shift of the emission. In addition, this spectral shift is relatively insensitive to variations in protein concentrations and interference due to light-scattering. Since the magnitude of the shift varies for different domains, depending on the fraction of tryptophan residues initially exposed at the start of the transition, the curves are normalized to the signal measured at the lowest (0) and the highest (1) concentration of denaturant. However, these normalized values do not correspond to the fraction of molecules unfolded, since the different domains do not contribute equally to the fluorescence signal and no baseline correction was applied to the curves.

As a consequence, we do not attempt to derive  $\Delta G_{H2O}$  values for the different transitions, since even global-fit algorithms do not produce robust fits for the, at least three, states we can clearly discern in many of the curves. The fits are particularly unreliable in the cases where the two transitions in a presumed three-state or higher equilibrium system are so close to each other that the resulting curve cannot be distinguished clearly from a two-state unfolding curve with lower cooperativity. Further problems arise when the spectral properties of the presumed intermediate cannot be observed directly, but have to be derived from the fit. It is also less straightforward to estimate the difference between  $\Delta G_{NU(H2O)}$  values for constructs of different sizes. For point mutations within a molecule it can often be assumed that the *m*-value, relating  $\Delta G_{NU}$  to the concentration of denaturant, is not affected by the mutation. This clearly does not hold true when comparing constructs of different sizes. Since the *m*-value is roughly proportional to the area of hydrophobic surface exposed upon unfolding,<sup>44</sup> we expect the dependence of  $\Delta G_{NU}$  on the concentration of denaturant to become steeper for larger constructs, and a shift in the denaturant midpoint not to be proportional to  $\Delta \Delta G_{NU}$  for different constructs at zero denaturant concentration. In other words, constructs with very different  $\Delta G_{NU(H2O)}$  values can have the same  $GdnHCl_{50}$ , if they have very different molecular masses, and therefore different *m*-values.

### Kinetic stabilization

For isolated domains and scFv fragments, the unfolding (starting from native protein) and refolding (starting from fully denatured protein) reactions reached equilibrium within 12 hours, as shown by the coincidence of the two curves. In contrast, the  $C_HC_S^{SS}$  heterodimer took two weeks to reach equilibrium. Fab and Fab<sup>SS</sup> fragments could not be refolded quantitatively from the fully denatured state, and thus the difference between denaturation and renaturation curves could not be used to monitor the approach to equilibrium. However, it took nearly a month of equilibration until no further

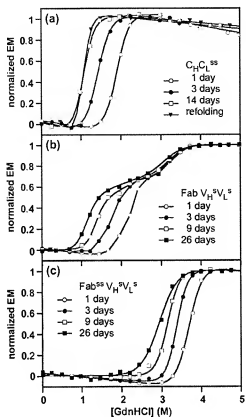


Figure 2. Time-course of unfolding transition curves. To follow the slow unfolding of the  $C_{14}C_{25}$ , Fab  $V_H^{55}V_L^5$  and Fab $^{55}V_H^5V_L^5$  fragments, samples were prepared from a protein stock solution without denaturant and mixed with increasing amounts of GdnHCl. The samples were incubated at 20 °C for the time indicated in the plot and their fluorescence emission spectra determined. Unfolding curves were plotted as normalized emission maxima (EM) as a function of denaturant concentration. Increasing incubation times shift the midpoints of unfolding towards a lower concentration of GdnHCl. (a) For the  $C_{14}C_{25}$  fragment, no further shift was observed after 14 days (□) and the curve is superimposable with the refolding curve (▼), indicating that equilibrium was reached. (b) and (c) For the Fab and Fab $^{55}$  fragments, no refolding curve could be measured due to incomplete reversibility.

change in the denaturation curve could be discerned (Figure 2).

#### Interface interaction

We begin our analysis with constructs composed of two domains (Figures 1 and 3), in order to gain insight into the effect on mutual stabilization of the individual domains across various interfaces. In the case of the scFv  $V_H^{55}V_L^5$  fragment, a strong stabilizing effect of the  $V_H/V_L$  interface is observed.<sup>17</sup> The denaturation curve of the scFv  $V_H^{55}V_L^5$  fragment (Figure 3(a)) follows a two-state model, indicated by

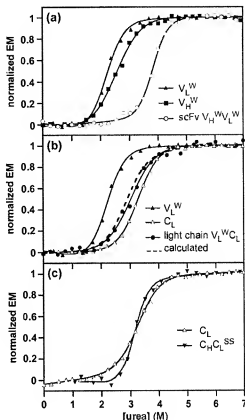


Figure 3. Equilibrium denaturation curves of the different two-domain assemblies compared with their constituent domains. Normalized curves are shown to facilitate the comparison of the unfolding transitions. The EM normalization makes no assumption about pre-transition or post-transition baselines. The continuous lines provided in all plots do not correspond to a two-state or a three-state fit, but are supplied for guidance. In (a), a significant shift of the unfolding transition towards a higher concentration of urea is observed for the scFv  $V_H^5V_L^5$  fragment (○) as compared to its constituent domains  $V_H^5$  (■) and  $V_L^5$  (▲). (b) The equilibrium denaturation curve (■) of the light chain (●), in contrast, corresponds almost perfectly to the unfolding curve (---) calculated from the sum of the spectra of the two constituent domains  $V_H^5$  (▲) and  $C_L$  (△) at the different denaturant concentrations. (c) In the light of the slow unfolding rate of the  $C_{14}C_{25}$  fragment (▼), the refolding curve, starting from a protein stock solution in 6.5 M urea, is shown. A steeper transition indicates higher cooperativity for the equilibrium denaturation curve of the  $C_{14}C_{25}$  fragment (▼) than for the isolated  $C_L$  domain (△) and the light chain (●).

a cooperative unfolding of the two domains, with a denaturation midpoint higher than that of the individual domains. This suggests that in the scFv fragment, the  $V_H^5$  and  $V_L^5$  domains interact strongly, and that through this interaction the two domains are stabilized to such an extent that the scFv unfolds

as a unit that is significantly more stable than either of the constituent domains.

In the case of the whole light chain, composed of a  $V_L$  domain and a  $C_L$  domain, the unfolding curve of the two-domain assembly is identical with the unfolding curve calculated from the weighted sum of the spectra of the two isolated domains at the different concentrations of denaturant (Figure 3(b)), which is consistent with previous observations.<sup>45</sup> This result demonstrates that no significant stabilizing interactions occur between the  $V_L$  and  $C_L$  domain, as expected from the small  $V_L/C_L$  interface within one chain. Unfortunately, the corresponding experiment could not be carried out for the Fd part of the heavy chain, since aggregation or multimerization occurred in the transition of unfolding. This behavior has been observed for other Fd chains.<sup>46</sup> However, we assume that the situation is similar to that for the light chain, because of its similar structural arrangement. Early experiments studying the limited papain cleavage of Fd fragments generated from rabbit IgG are consistent with the view that  $V_H$  and  $C_H$  domains do not interact strongly in the absence of the light chain, but are linked through a flexible, protease-sensitive connection.<sup>47</sup>

In the case of the  $C_{H1}V_L^{SS}$  heterodimer, the renaturation midpoint of the two-domain construct coincided with the midpoint of the unfolding transition of the isolated  $C_{H1}$  domain (Figure 3(c)), although the unfolding reaction was much slower for the two-domain construct. It took two weeks of incubation until the reaction was sufficiently close to equilibrium for the midpoint of the denaturation curve to coincide with that of the renaturation curve (Figure 2(a)). Because of the weak interface interaction between the  $C_{H1}$  and  $C_L$  domains, we had to use the disulfide-bonded version in order to obtain a homogenous protein preparation. As expected<sup>44</sup> for the larger size of the  $C_{H1}C_L^{SS}$ , its  $m$ -value was higher than that of the isolated  $C_L$  domain (Figure 3(c)). In contrast to the whole light chain, a sharp transition is observed for the  $C_{H1}V_L^{SS}$  fragment, indicating cooperative unfolding and therefore strongly interacting domains. Since the  $C_{H1}$  domain cannot be studied (as it is insoluble or unstable in the absence of the  $C_L$  domain), we have no data to describe its unfolding, but we can assume that the intrinsic stability of the  $C_{H1}$  domain is not higher than that of the  $C_L$  domain. Otherwise, it would shift the midpoint of unfolding of the  $C_{H1}C_L^{SS}$  fragment to a higher concentration of denaturant. Thus, while no significant domain interaction at the  $V_L/C_L$  interface is observed, the  $V_H/V_L$  and  $C_{H1}/C_L$  interfaces show mutual interactions, which lead to cooperative unfolding of the domain pairs.

#### From isolated domains to the Fab fragment

In a second series of experiments (Figure 4), the influence of the constant domains on the variable domains in the Fab format was studied by assembling the Fab in a stepwise manner. The

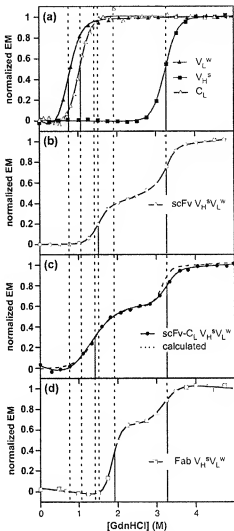


**Figure 4.** Comparison of the unfolding transitions of the scFv  $V_H^S V_L^W$  fragment ( $\circ$ ), (b)), the scFv- $C_L$   $V_H^S V_L^W$  fragment ( $\bullet$ ), (c)), the Fab  $V_H^S V_L^W$  fragment ( $\square$ ), (d)) and (a) their constituent isolated domains  $V_L^W$  ( $\blacktriangle$ ),  $V_H^S$  ( $\blacksquare$ ) and  $C_L$  ( $\triangle$ ). Upon addition of one (scFv- $C_L$ ) and two (Fab) constant domains, the plateau of the emission maximum, corresponding to a folding intermediate, is shifted to a higher wavelength. This shift indicates a higher proportion of tryptophan residues exposed to the solvent for these constructs. The scFv- $C_L$   $V_H^S V_L^W$  fragment ( $\bullet$ ) shows an earlier onset of unfolding than the corresponding scFv, presumably due to the  $C_L$  domain ( $\triangle$ ), which is not stabilized in this construct. However, as soon as both constant domains are present in the Fab  $V_H^S V_L^W$  fragment ( $\circ$ ), a shift of the first transition towards a higher concentration of GdnHCl and a highly cooperative unfolding is observed.

denaturation curves of the isolated domains are shown in Figure 4(a). Variable domains ( $V_H^S$  and  $V_L^W$ ) with significantly different intrinsic stabilities were combined to yield the scFv  $V_H^S V_L^W$  fragment

(Figure 4(a) and (b)). This difference in stability leads to two distinct unfolding transitions for the two variable domains in the scFv format and, therefore, to an unfolding intermediate for the denaturation of the scFv fragment (Figure 4(b)). Thus, the influence of the constant domains on these variable domains can be observed individually. In this scFv  $V_H^S V_L^W$  fragment, the midpoint of the first transition lies at a higher concentration of denaturant than the denaturation midpoint of the isolated  $V_L^W$  domain, indicating stabilization of the  $V_L^W$  domain by its interaction with the more stable  $V_H^S$  domain. The second transition, which remains unchanged, reflects the unfolding of the more stable domain,  $V_H^S$ , in the scFv fragment. Like in the scFv  $V_H^S V_L^W$  fragment (Figure 3(a)), a stabilizing effect is observed at the  $V_H^S/V_L^W$  interface.

In the next step, we fused the  $C_L$  domain to the  $V_L$  domain in the scFv format to give the three-domain assembly scFv- $C_L$   $V_H^S V_L^W$ . A  $C_L$  domain added to the C terminus of an scFv fragment in  $V_H^S$ -linker- $V_L$  orientation had no effect on the thermodynamic stability of either the scFv fragment or the  $C_L$  domain (Figure 4(a)–(c)). The unfolding curve of the three-domain assembly is identical with the calculated sum of the unfolding curves of the isolated  $C_L$  domain and the corresponding scFv fragment (Figure 4(c)), similar to what was observed for the light chain  $V_L C_L$  (Figure 3(b)). While it has been reported that the addition of a  $C_L$  domain can increase the functional half-life of some scFv intrabodies in the cytoplasm and nucleus of eukaryotic cells,<sup>48–50</sup> this most probably is not due to altered thermodynamic stability, but to reduced *in vivo* aggregation and/or degradation of the construct.

Finally, by adding the  $C_{H1}$  domain, the complete Fab  $V_H^S V_L^W$  fragment is generated. In contrast to the scFv and the scFv- $C_L$  fragments, which are linked via a peptide linker, the light and the Fd chain of the Fab  $V_H^S V_L^W$  fragment are held together by non-covalent interactions. Still, two transitions are observed for this construct. While the second transition remains unchanged as compared to the scFv  $V_H^S V_L^W$  and scFv- $C_L$   $V_H^S V_L^W$  fragment, the first transition occurs at a higher concentration of denaturant. Thus, both the unfolding of the  $V_L^W$  domain and of the constant domains is further shifted to a higher concentration of denaturant. This result demonstrates clearly that both constant domains are required for a further stabilization of both variable and constant domains.

#### Influence of variable domain stability on the Fab fragment stability

The weakest of the scFv fragments tested in this analysis, composed of a  $V_H^W$  and a  $V_L^W$  domain, shows a  $GdnHCl_{50}$  of 1.4 M, compared to the  $C_H C_L^{SS}$  heterodimer with a  $GdnHCl_{50}$  of 1.1 M (Figures 5(a) and 2(a)). Of course, this does not necessarily translate to a higher  $\Delta G$  of unfolding in the absence of denaturant for the scFv fragment, as a broader

transition of the scFv fragment denaturation curve suggests that the scFv fragment may not truly follow a two-state model. The non-disulfide-linked Fab  $V_H^S V_L^W$  fragment, composed of the same four domains as discussed, shows a highly cooperative unfolding curve with a  $GdnHCl_{50}$  of 1.9 M, indicating significant mutual stabilization between the  $V_H^S V_L^W$  and the  $C_H C_L$  heterodimer (Figure 5(b)).

If the stability of the  $V_H^S$  domain in the scFv fragment is increased by re-introduction of the intradomain disulfide bond, the difference between the intrinsic stabilities of the weak  $V_L^W$  domain with a  $GdnHCl_{50}$  of 0.8 M and the  $V_H^S$  domain with 3.2 M becomes too large for a single cooperative unfolding transition. As a consequence, the unfolding curve of the scFv fragment shows two distinct unfolding transitions upon increasing the concentration of denaturant (Figure 5(c)). The first transition represents the unfolding of the  $V_L^W$  domain, which, with a  $GdnHCl_{50}$  of 1.5 M, is stabilized significantly by its interaction with the strong  $V_H^S$  domain. The second domain ( $V_H^S$ ) unfolds with a  $GdnHCl_{50}$  of 3.2 M, and thus at the same  $GdnHCl$  concentration as in isolation.<sup>51</sup> If we convert this scFv to a Fab fragment, we again get two transitions (Figure 5(d)); the first at a  $GdnHCl_{50}$  of 1.9 M (representing the unfolding of  $V_L^W$ ,  $C_L$  and  $C_{H1}$ ) and the second at 3.2 M (representing the unfolding of the  $V_H^S$  domain). Thus, the unfolding of the  $V_L^W$  domain is further shifted to higher concentrations of denaturant, as compared to the same domain in the context of an scFv fragment. As the  $V_L^W$  domain unfolds, the Fv part of the Fab fragment is no longer able to stabilize the constant domains, and only the  $V_H^S$  domain remains folded. Therefore, we conclude that the  $C_H C_L$  heterodimer unfolds along with the  $V_L^W$  domain. Introduction of a disulfide bond connecting the C termini of the two chains further shifts the first unfolding transition to a higher concentration of denaturant ( $GdnHCl_{50}$  2.4 M), while the second transition is unchanged (Figure 5(e)).

For the third series of scFv/Fab/Fab<sup>SS</sup> fragment comparisons (Figure 5(f)–(h)), the very weak  $V_L$  domain of ABPC48 ( $V_L^W$ ) was replaced by the very stable  $V_L$  domain ( $V_L^S$ )<sup>52</sup> of the antibody 4D5.<sup>52</sup> With a  $GdnHCl_{50}$  of 2.7 M, this  $V_L^S$  domain approaches the stability of the  $V_H^S$  domain. Therefore, the unfolding behavior of this single-chain fragment again resembles a two-state process, albeit with a slightly lower midpoint (3.05 M) than that of the isolated  $V_H^S$  domain (3.2 M) (Figure 5(f)). Since we replaced a murine  $V_{\kappa 10}$  domain by a human  $V_{\kappa 1}$  domain, there were some sequence differences located within the  $V_H^S/V_L^S$  interface, and we can no longer assume the  $V_H^S/V_L^S$  interaction to be exactly the same as in the two other scFv fragments. A weakened  $V_H^S/V_L^S$  interface may offer some explanation for the unexpectedly low  $GdnHCl_{50}$  (1.1 M) of the first unfolding transition in the Fab fragment, which corresponds to the unfolding of both constant domains (Figure 5(g)). Although we

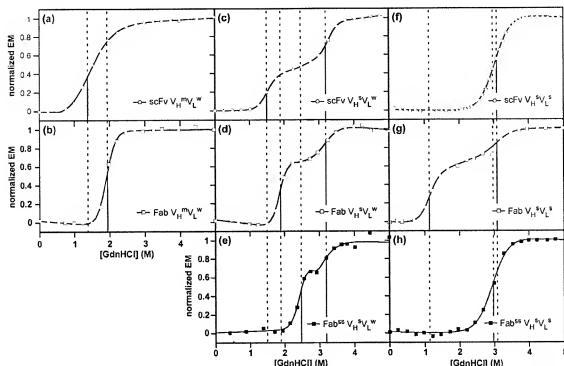


Figure 5. Comparison of the scFv fragments (○), Fab fragments (□) and Fab<sup>SS</sup> fragments (■) consisting of different variable domain combinations (V<sub>H</sub>V<sub>L</sub> left panel, V<sub>H</sub><sup>ss</sup>V<sub>L</sub> middle panel, V<sub>H</sub><sup>ss</sup>V<sub>L</sub> right panel). While the Fab V<sub>H</sub>V<sub>L</sub>, Fab V<sub>H</sub><sup>ss</sup>V<sub>L</sub> and Fab<sup>SS</sup>V<sub>H</sub>V<sub>L</sub> fragments were incubated for 14 days, the Fab V<sub>H</sub><sup>ss</sup>V<sub>L</sub> and Fab<sup>SS</sup>V<sub>H</sub><sup>ss</sup>V<sub>L</sub> fragments were incubated for 26 days at 20 °C before measurements. The normalization applied to the data makes no assumption about pre-transition or post-transition baselines. Note that the continuous lines are supplied simply for guidance and do not represent a fit.

see no evidence of premature domain dissociation in the scFv fragment, the linker may keep these intrinsically stable domains at high local concentration in the scFv fragment, which is not the case in the Fab fragment lacking the interchain disulfide bridge. As Figure 2(b) shows, the unfolding of the C<sub>H</sub>C<sub>I</sub> heterodimer within the Fab fragment, which occurs at lower concentrations of denaturant than that of the V<sub>H</sub>V<sub>L</sub> heterodimer, is observed already at the earliest time-points measured. Introduction of the C-terminal disulfide bond stabilizes the Fab fragment to the point where it shows an unfolding curve very similar to that of the scFv fragment (Figure 5(f) and (h)), but with the very slow unfolding kinetics of the C<sub>H</sub>C<sub>I</sub> heterodimer (Figure 2(c)). This construct combines the high-level stability of an scFv fragment composed of very stable variable domains with the kinetic stabilization of a Fab<sup>SS</sup> fragment. We find that this superior stability (both thermodynamic and kinetic) is strictly dependent on the presence of the interchain disulfide bond (Figure 5(d) and (e) or (g) and (h)). We find that the C<sub>H</sub>1 and C<sub>I</sub> domains are mostly a liability in the case of very stable V<sub>H</sub> and V<sub>L</sub> domains (Figure 5(f) and (g)), in the absence of an interchain disulfide bond.

## Discussion

### Multidomain proteins

Multidomain proteins can show complex equilibrium unfolding behavior. At one extreme we find proteins consisting of multiple, non-interacting domains, which are connected covalently by flexible linker sequences. These domains will unfold sequentially upon increasing temperature or concentration of denaturant, according to their intrinsic stability (stability in the absence of interactions with any other folded domain). The equilibrium unfolding curve of such a protein can be represented as the sum of the unfolding transitions of the individual domains. At the other extreme are assemblies whose domains interact so strongly that no single domain can unfold without all the other domains unfolding as well. Such multidomain proteins show a single two-state unfolding transition, similar to a single-domain protein, and the overall protein stability is higher than that of any of the constituent domains in isolation.

Between these two extremes lie the multidomain assemblies, in which some of the constituent domains are stabilized significantly by their

interactions with other domains, but not stabilized sufficiently to enforce a fully cooperative unfolding transition. The unfolding behavior of such proteins can be described by a model in which the stability of each domain within the multidomain assembly is the sum of its intrinsic stability and the additional stabilization it experiences through its interactions with neighboring folded domains.<sup>53</sup> This additional stabilization is reduced to zero as soon as either of the interacting domains unfolds, since it is dependent on the structural integrity of the interacting domains. Such mutual stabilization of domains can occur between domains within a single polypeptide chain, between domains on different chains connected by a disulfide linkage or between non-covalently associated domains. If the interacting partners are not connected covalently, the interaction terms become concentration-dependent.<sup>54</sup>

### Geometry of domain interactions

This model of interdomain stabilization has been tested with a series of scFv fragments. Different equilibrium unfolding behavior, depending on the relative magnitudes of the intrinsic stabilities of the domains and the interaction terms, were observed.<sup>57,55</sup> In the present study, we extended this analysis from the two-domain scFv system to a four-domain system, the Fab fragment. In the Fab fragment, we find two distinct types of interfaces: the  $V_H/V_L$  and  $C_{H1}/C_{L1}$  interfaces are large, densely packed, and predominantly hydrophobic. These interfaces (Figure 6(a)) allow only limited flexibility in the relative orientation of the domains (Figure 7(c)). In contrast, the  $V_H/C_H$  and the  $V_L/C_L$  interface are packed only loosely (Figure 6(b)), and there is a high degree of flexibility in the relative orientation of the  $V_H/V_L$  heterodimer against the  $C_{H1}/C_{L1}$  heterodimer (Figure 7(a) and (b)). The elbow angle, defined as the angle between the pseudo-dimer axes of the two heterodimers, was found to be between 127° and 227°.<sup>56</sup> It appears to depend more on crystal packing than on local sequence features, as it also varies between multiple copies of the Fab fragment in the asymmetric unit of a crystal<sup>57,58</sup> and between the two Fab fragments within an intact IgG molecule.<sup>59</sup>

On average,  $1570(\pm 160)$  Å<sup>2</sup> of solvent-accessible surface get buried upon formation of the  $V_H/V_L$  interface, and 70% of this surface is non-polar (analysis of >200 Fab structures, using the program NACCESS†). The  $C_{H1}/C_{L1}$  interface buries  $1970(\pm 160)$  Å<sup>2</sup> of solvent-accessible surface, 70% of it non-polar. The total contact area between the light chain and the Fd fragment of the heavy chain therefore amounts to  $3540(\pm 220)$  Å<sup>2</sup>, 70% of it apolar. In contrast, the  $V_L/C_L$  and  $V_H/C_H$  interfaces are small:  $410(\pm 190)$  Å<sup>2</sup> buried for  $V_L/C_L$ ,  $800(\pm 100)$  Å<sup>2</sup> (43% non-polar) for  $V_H/C_H$  and

$390(\pm 70)$  Å<sup>2</sup> (57% non-polar) for the  $V_H/C_H$  interface. This results in a total of  $1220(\pm 180)$  Å<sup>2</sup>, of which 48% are non-polar, for the interface between the  $V_H/V_L$  heterodimer and the  $C_{H1}/C_{L1}$  heterodimer in Fab fragments containing a κ light chain. The interfaces between the variable and the constant domains are loosely packed and no more hydrophobic than the average total accessible surface of the Fab fragment ( $19,500(\pm 420)$  Å<sup>2</sup>, 54% of the area non-polar) (Figure 6).

### Intermolecular disulfide bond

Since the interchain disulfide bond at the C-terminal ends of the constant domains plays an important role in the stabilization of the Fab fragment (Figure 5), we analyzed its occurrence in different Ig families. Human and murine light chains have a cysteine residue at the C terminus of the chain (L214). λ light chains have a cysteine residue in the penultimate position (L214). This cysteine residue can, in most antibodies, participate in a disulfide bond connecting the light chain and the heavy chain (Figure 8). However, while every heavy chain provides a potential partner, its position is less conserved than that of the light chain cysteine residue (Figure 8(a)): it may be either a cysteine residue in position H233 (the first cysteine residue of the hinge exon in IgG1) or a cysteine residue in position H127 or H128 of the heavy chain, located in the loop between the first and the second strand of the  $C_{H1}$  domain (present in all human and murine  $C_{H1}$  domains except IgG1 and human IgA2). A special situation exists in IgAs, where formation of an intradomain disulfide bond between the simultaneously present CysH127 and CysH223B (human IgA1) or between CysH198 and CysH223B (human and murine IgAs) may prevent the formation of the interchain disulfide bond. Both the loop containing the cysteine residue in positions H127 or H128 and the residues around CysH123 are very flexible, as indicated by high B-factors of these residues within individual structures, by a high degree of divergence between different structures (Figure 8(b)) and a large number of structures in which these residues are not resolved. Of 280 Fab fragment X-ray structures analyzed, 30 carried a visible disulfide bond connecting the C-terminal ends of  $C_L$  and  $C_{H1}$ , and 60 carried a disulfide bond connecting a cysteine residue in position H127 or H128 with the cysteine residue in the  $C_L$  domain. In 190 Fab fragments, no interchain disulfide bond was found, either because the cysteine residues were missing or too poorly resolved to be visible in the structure or, in rarer cases, because both cysteine residues were visible but too far apart to be linked by a disulfide bond.

To assess the effect of the  $C_{H1}$  domain type and of the interchain disulfide bond on the relative orientation of the  $C_{H1}$  against the  $C_L$  domain, we analyzed this relative orientation in >200 human and murine  $C_{H1}/C_{L1}$  pairs excised from Fab fragment structures. To illustrate the high conservation

† <http://wolf.bms.umist.ac.uk/naccess/>

# EXHIBIT B

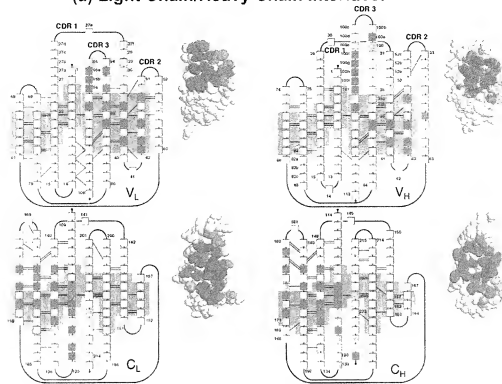
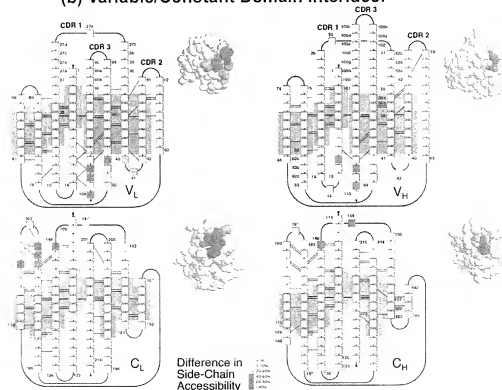
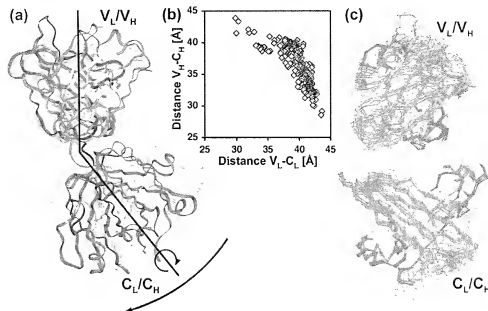
**(a) Light Chain/Heavy Chain Interface:****(b) Variable/Constant Domain Interface:**

Figure 6 (legend opposite)



**Figure 7.** Flexibility of the relative orientations of the domains within the Fab fragment. (a) Three Fab fragments were superimposed by a least-squares fit of the structurally least variable  $C^{\alpha}$  positions within the Fv part (indicated in white) to illustrate the flexibility of the variable/constant domain interface. (b) Plot of the distance between the centers of gravity of  $V_H$  and  $C_{H1}$  versus the distance between the centers of gravity of  $V_L$  and  $C_L$ . Only the structurally conserved  $C^{\alpha}$  positions (indicated by a gray background in Figure 6) were used for the calculation of the center of gravity. The observed anti-correlation is explained by a twist around the  $C_{H1}/C_L$  pseudo 2-fold axis. (c) Limited flexibility of the  $V_H/V_L$  and of the  $C_L/C_H$  interface, demonstrated by structurally aligning the  $V_L$  and  $C_L$  domains, respectively. From the comparison of (a) and (c), it becomes apparent that  $V_H/V_L$  and  $C_{H1}/C_L$  are each moving as a unit.

of the relative domain orientation, we show a superposition of the best-resolved structures in Figure 7(c). The  $C_K/C_{K1}$  pairs were superimposed by a least-squares fit of the structurally most conserved  $C^{\alpha}$  atoms of the  $C_K$  domains (indicated by the gray underlay in Figures 6 and 8(a) and shown white in the aligned structures). Clearly, the relative domain orientation is highly conserved, although the position of the interdomain disulfide bond is not. Taken together, the structures indicate great structural flexibility of the first loop connecting strands a and b, the C-terminal residues of the heavy chains (strand g) and the beginning of the hinge region (Figure 8(b)). Therefore, the  $C_{H1}/C_L$  pair is a tight unit (Figure 7(c)), but the disulfide bond is only a somewhat mobile tether.

#### Influence of different V-domains on the stability of scFv and Fab fragments

The variable domains ( $V_H^W$ ,  $V_H^M$ ,  $V_H^S$  and  $V_L^W$ ,  $V_L^M$ ) analyzed in this study and the scFv fragments ( $V_H^WV_H^M$ ,  $V_H^WV_L^M$ ,  $V_H^MV_L^M$  and  $V_H^SV_L^M$ ) derived from them have been characterized.<sup>55,60</sup> They are shown to be sufficiently stable for production and analysis, while at the same time covering a wide range of biophysical behavior. ScFv fragments less stable than the weakest of these scFv fragments are not uncommon, but we chose to work with fragments sufficiently stable for detailed characterization of the constituent domains as well as the scFv and Fab fragments. In the scFv  $V_H^WV_L^M$  and  $V_H^WV_L^S$  fragment, the two domains show significant mutual

**Figure 6.** Interdomain interfaces. The average contribution of each residue's position to the different interfaces in 30 non-redundant Fab fragments (25 with a  $\kappa$ , five with a  $\lambda$  light chain) has been assessed by calculating the solvent-accessible surface of each residue in the Fab fragment, in  $V_LV_H$ ,  $C_LC_H$ ,  $V_LC_L$  and  $V_HC_H$  pairs and in the isolated domains, using the program NACCESS (<http://wolf.bms.umist.ac.uk/naccess/>). From these values, the average relative loss of accessible surface area upon interface formation was calculated for each position in the Fab fragment. The numeric values were converted to a color code and projected onto a schematic representation and a spacefilling representation of the  $V_L$ ,  $V_H$ ,  $C_L$  and  $C_H$  domains taken from a representative antibody structure (PDB entry 1IGT). Side-chains whose solvent-accessible surface area, on average, is not affected significantly by the association of the domains (less than 1% difference) are in white; slightly affected ones (1–20%) yellow; 40–60% reduction in accessible surface area, orange; 60–80% difference, red-orange; and >80% difference, red.

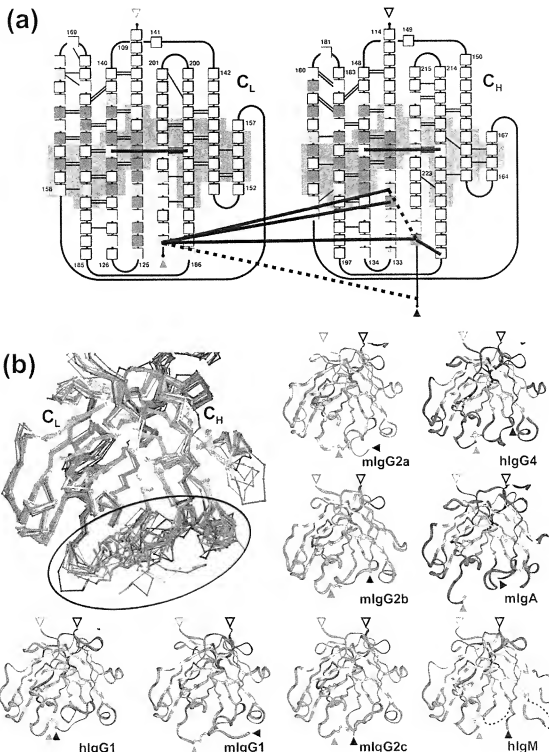


**Figure 8.** Flexibility of the interdomain disulfide bond. (a) A representation of a C<sub>H</sub>1 and a C<sub>L</sub> domain. The color code of the boxes representing the atom positions indicates the contribution of the side-chains of these residues to the C<sub>H</sub>1 + C<sub>L</sub> interface as described in the legend to Figure 6. Continuous, thick black lines indicate different disulfide linkages that have been observed in Fab structures, broken lines indicate additionally possible disulfide bonds. For details, see the text. (b) Structural flexibility in the region containing the interchain disulfide bonds. An overlay of representative, well-resolved structures of the constant domains from Fab fragments from different immunoglobulin isotypes illustrates both

stabilization. In the scFv  $V_H^*$  $V_L^*$  fragment, the weak  $V_L^*$  domain was stabilized significantly while still unfolding at a lower concentration of denaturant than the isolated  $V_L^*$ . Finally, in the strongest scFv fragment,  $V_H^*$  $V_L^*$ , a denaturation midpoint between that of the isolated  $V_L^*$  and that of the isolated  $V_H^*$  domain in an apparent two-state unfolding curve, albeit with a broader transition, indicated a borderline case between two-state and three-state unfolding behavior.

The C-terminal fusion of just the  $C_L$  domain to the scFv  $V_H^*$  $V_L^*$  fragment had no effect on its stability. The unfolding curve calculated from the spectra of the scFv- $C_L$ ,  $V_H^*$  $V_L^*$  fragment could be superimposed with the curve calculated from the sum of the spectra of scFv fragment and isolated  $C_L$  domain at the different concentrations of denaturant. This agrees with expectations based on the very limited interaction interface between the  $V_L$  and  $C_L$  domains and with earlier observations of the stabilities of Fv, Fv- $C_L$  and Fab fragments.<sup>28</sup> In this reported study the chains were not linked covalently. The melting temperature of the reported Fab fragment was found to about 15 °C higher than that of the Fv fragment, and no significant difference was observed between the Fv fragment with or without the additional  $C_L$  domain. This result was consistent with hydrogen/deuterium exchange determinations of the Fv and Fab fragment of the same antibody.<sup>31</sup> Therefore, the authors came to the conclusion that both constant domains  $C_H1$  and  $C_L$  are necessary for the stabilization of the variable domains. However, with a wide range of Fab fragments, we now find that this stabilization is true only for weak or medium stable variable domains. In the case of very stable variable domains in both the heavy and light chain, the constant domains become limiting. Only in the presence of disulfide-linked constant domains do Fab fragments with very stable variable domains reach the stability of the stable scFv fragments.

### $V_HV_L$ and $C_HC_L$ each form a unit

The interaction interface between  $V_H$  and  $C_H1$  is even smaller than that between  $V_L$  and  $C_L$ , and we can therefore safely assume that there is as little direct mutual stabilization between  $V_H$  and  $C_H1$  as between  $V_L$  and  $C_L$ . However, the situation is very different for the whole Fab fragment with its two chains. We clearly observe a high degree of mutual stabilization between the  $V_HV_L$  heterodimer and the  $C_HC_L$  heterodimer. This is not simply a case of a weak  $V_HV_L$  heterodimer being stabilized by a much stronger  $C_HC_L$  heterodimer. Rather, the intrinsic stability of the constant domains is in the same range as that of a very weak variable domain. Despite the larger hydrophobic interaction area between  $C_H1$  and  $C_L$  than that between  $V_H$  and  $V_L$ , the affinity between the two isolated constant domains is too low for them to remain associated throughout purification in the absence of a covalent linkage. Stabilization of the  $C_HC_L$  heterodimer by domain association and the introduction of an interchain disulfide bond appear to increase the activation barrier for unfolding rather than to increase the equilibrium stability. Nevertheless, the  $C_H1$  domain, which cannot be expressed and studied well in isolation, obviously experiences some interface stabilization. The equilibrium stability of the  $C_HC_L^{S2}$  heterodimer is still relatively low (Figure 2(a)), but is increased significantly by the interaction with a  $V_HV_L$  heterodimer (Figure 5).

The geometry of the interaction between  $C_H1$  and  $C_L$  is very different from that of the interaction between  $V_H$  and  $V_L$  (Figure 6). Not only does it use the other  $\beta$ -sheet of the  $\beta$ -sandwich, but the two  $\beta$ -sheets forming the  $C_H1/C_L$  interface are placed at an almost right-angle to each other, while the two  $\beta$ -sheets of the  $V_H/V_L$  interface together resemble a  $\beta$ -barrel filled by mostly hydrophobic residues. It is not clear why the large and hydrophobic  $C_H1/C_L$  interface does not lead to a very strong interaction in the absence of the interdomain disulfide bond.

---

the conservation of the overall structure and the structural flexibility of the C termini and loops involved in interchain disulfide linkage. The N termini of the domains are indicated by open triangles, the C termini by filled triangles, gray for  $C_L$  and black for  $C_H1$ . This flexible region is as structurally divergent between structures of Fab fragments of the same isotype (e.g. murine IgG1) as it is between the different isotypes. In many of the Fab fragments analyzed, the C terminus of the  $C_H1$  domain and some of the loops in this regions have not been resolved. Human IgG1s are represented by PDB entry 1NGZ (1.6 Å resolution, no interchain disulfide bond visible, red) and PDB entry 1L7I (1.8 Å resolution, with a C-terminal disulfide bond linking CysL214 to a C-terminal cysteine residue, red). Murine IgG1 is represented by PDB entries 1NLB (1.6 Å resolution, no interchain disulfide bond, orange) and 1WEJ (1.8 Å resolution, with a C-terminal disulfide bond, orange). Murine IgG2a is represented by PDB entries 1NBY (1.8 Å resolution, no disulfide bond, yellow) and 1NCW (1.3 Å resolution, disulfide bond between the terminal CysL214 and CysH128, yellow), murine IgG2b by 1OSP (1.92 Å resolution, no disulfide bond, yellow-green) and 1NBV (2.0 Å resolution, disulfide bond between CysL214 and CysH128, yellow-green), and murine IgG2c by 1HIL (2.0 Å resolution, no interchain disulfide bond, green) and 1H16 (2.55 Å resolution, disulfide bond between CysL214 and CysH128, green). Murine IgG3 is represented by PDB entry 1KCV (1.8 Å resolution, no interchain disulfide bond, light blue), human IgG4 by PDB entry 1AD0 (2.5 Å resolution, no interchain disulfide bond, dark blue). PDB entry 2FBj (1.95 Å resolution, no interchain disulfide bond, purple) represents the murine IgA, which has an additional interchain disulfide bond linking CysT198 and CysH223B. PDB entry 1QLR (2.83 Å resolution, magenta) represents the human IgM and has an interchain disulfide bond linking CysL214 to CysH127. Individual structures are shown for those representative structures of each isotype where the interchain disulfide bond is present.

Perhaps this interface is too rigid to be able to adapt. In the presence of the interdomain disulfide bond, on the other hand, a remarkable kinetic stabilization against unfolding is observed. This implies that the concerted motions needed for domain unfolding are optimally blocked by the other domain being "in the way". This is not the case for the variable domains, which reach equilibrium rapidly. In the constant domains, all strands of one sheet and one strand of the other are involved strongly in the interdomain interaction. It is possible that a "peeling" of the edge strands is therefore more difficult.

While the mutual stabilization at the  $V_H/V_L$  or  $C_{H1}/C_L$  interface relies on the formation of a large, well-packed hydrophobic interdomain interface, this is not the case for the mutual stabilization between the  $V_H/V_L$  and  $C_H/C_L$  heterodimers. Even if we assume a high degree of cooperativity between the formation of the  $V_H/C_{H1}$  interface and the  $V_L/C_L$  interface, these two small, poorly packed, and rather hydrophilic interfaces would contribute minimally to stability. The mutual stabilization of  $V_{H1}V_L$  and  $C_{H1}C_L^{ss}$  heterodimers relies not on the formation of a tightly packed interface, but on the fixed distance and orientation of the two C-terminal ends of the variable domain for the stabilization of the  $V_H/V_L$  heterodimer and, *vice versa*, for the two N-terminal ends of the  $C_{H1}C_L^{ss}$  heterodimer. Each of the domain pairs thus acts as an optimal linker for the other, strengthening the association of  $V_H$  with  $V_L$  and of  $C_{H1}$  with  $C_L$  through their respective heterodimer interfaces. This interface stabilization is enhanced strongly by the presence of the disulfide bond connecting the C-terminal ends of the two constant domains preventing the dissociation of the  $C_H/C_L$  heterodimer. Without this disulfide bond, the stability of the  $C_H/C_L$  heterodimer becomes limiting for the stability of Fab fragments containing stable variable domains. In contrast, the midpoint of the unfolding transition of the  $C_{H1}C_L^{ss}$  heterodimer in the Fab fragment containing the strongest variable domains and an inter-chain disulfide bond is shifted to the level of the strong scFv fragment, and the variable domains in that Fab fragment profit from the kinetic stabilization of the  $C_H/C_L^{ss}$  heterodimer.

## Conclusions

In summary, Fab fragments extend the range of variable domains that can be used. Especially weak variable domains experience a considerable stabilization making them more useable for practical application. This effect is mostly due to kinetic stabilization provided by the  $C_H/C_L$  heterodimer and especially the disulfide-linked  $C_{H1}C_L^{ss}$  heterodimer. At equilibrium, the stabilizing effect is smaller. Conversely, with very stable variable domains, constant domains without an intra-domain disulfide bond become a liability. This is remedied only by the re-introduction of the

interdomain disulfide bond. The question of which format is "better", Fab fragment or scFv fragment, does not have a unique answer, but depends on the stability of the variable domains involved, as well as on the importance that is placed on production yields, as Fab fragments containing the interdomain disulfide bond tend to give lower yields in bacterial production than either Fab fragments without disulfide bond or scFv fragments. The production yield is a function of the different degrees of aggregation and degradation during folding in the cell. Increased understanding of the mechanisms of mutual domain stabilization will help in the design of even better antibody molecules.

## Materials and Methods

### Protein expression and purification

The isolated  $V_L^{ss}$  domain was expressed and purified as described.<sup>37</sup> The gene fragment for the  $C_L$  domain was inserted into the pLG vector.<sup>37</sup> The protein was expressed in soluble form in the periplasm of *E. coli* SB536,<sup>44</sup> and purified using a two-column coupled system (BioCAD). After the  $C_L$  domain was bound *via* the His-tag to the immobilized metal ion affinity chromatography (IMAC) column, it was washed with 1 M NaCl, eluted with 125 mM imidazole and loaded directly onto an anion-exchange column. The fragment eluted in pure form at the beginning of the applied salt gradient. The buffer was then exchanged to Mops buffer (20 mM Mops (pH 7), 150 mM NaCl) by dialysis.

To obtain the two-fragment assembly  $C_{H1}C_L^{ss}$ , the corresponding genes were inserted into the dicistronic vector pHJ290FF<sup>45</sup> expressed in the periplasm and purified as described above for the  $C_L$  domain. The light chain gene fragment was inserted into the pLG vector,<sup>37</sup> and expressed in soluble form in the periplasm of *E. coli* SB536.<sup>42</sup> For purification, the light chain was first applied to an IMAC column (BioCAD) and subsequently loaded onto a Superdex-75 size-exclusion column (Amersham Biosciences) in Mops buffer. The scFv fragments  $V_H^{ss}V_L^{ss}$  and  $V_H^{ss}V_L^{ss}$  were expressed and purified as described,<sup>37</sup> with the exception of using Mops buffer for the levan affinity column.

For the three-domain assembly scFv- $C_L$   $V_H^{ss}V_L^{ss}$ , the  $C_L$  domain gene was inserted behind the  $V_L$  domain to restore the natural light chain sequence in the expression vector for the scFv  $V_H^{ss}V_L^{ss}$  fragment. The dicistronic vector pHJ290FF<sup>45</sup> was used for the expression of the Fab fragments: Fab  $V_H^{ss}V_L^{ss}$ , Fab  $V_H^{ss}V_L^{ss}$ , Fab  $V_H^{ss}V_L^{ss}$  and Fab<sup>ss</sup>  $V_H^{ss}V_L^{ss}$ . The three-domain assembly scFv- $C_L$   $V_H^{ss}V_L^{ss}$  and all Fab fragments were expressed in soluble form in the periplasm of *E. coli* SB536.<sup>42</sup> Constructs containing the levan-binding site (the scFv- $C_L$   $V_H^{ss}V_L^{ss}$ , Fab  $V_H^{ss}V_L^{ss}$  and Fab<sup>ss</sup>  $V_H^{ss}V_L^{ss}$  fragments) were purified as described for the scFv  $V_H^{ss}V_L^{ss}$  fragment. The hybrid constructs between ABPC48 and 4D5 (the Fab  $V_H^{ss}V_L^{ss}$  and Fab<sup>ss</sup>  $V_H^{ss}V_L^{ss}$  fragments) were bound *via* the His-tag to the IMAC column and washed with 1 M NaCl. The protein was eluted with 30 mM imidazole (pH 8.5) and loaded directly onto an anion-exchange column. The Fab fragments eluted in pure form at the beginning of the applied salt gradient. The buffer was exchanged to Mops buffer by dialysis.

Protein concentrations were determined by measuring the absorption at 280 nm and using the calculated extinction coefficient.<sup>64</sup>

#### Equilibrium denaturation measurements

Using fluorescence spectroscopy, the unfolding or refolding of proteins was followed by monitoring a shift in emission maximum or in intensity at 330 nm or 350 nm for each concentration of denaturant. All fluorescence measurements were performed with a PTI Alpha Scan spectrofluorimeter (Photon Technologies Inc.), using an excitation wavelength of 280 nm and recording the emission spectra between 320 nm and 365 nm. The protein concentration was 0.2  $\mu$ M in all experiments. For equilibrium denaturation measurements, either native or completely denatured protein was incubated at 20 °C in Mops buffer containing various amounts of denaturant (urea or GdnHCl, respectively). Constructs containing both constant domains ( $C_1/C_2^{\text{ss}}$ , Fab and Fab<sup>ss</sup> fragments) were incubated for up to 26 days due to their slow unfolding. All other constructs were incubated overnight. While for isolated domains, two-domain and three-domain constructs, coincidence of the curves obtained starting from native protein (unfolding curve) and from fully denatured material (refolding curve) indicated that equilibrium had indeed been reached, dilution of fully denatured Fab fragments into low concentrations of GdnHCl leads to aggregation. Thus, Fab and Fab<sup>ss</sup> denaturation was deemed to have reached equilibrium when no further shift of the midpoint of the unfolding curve with increasing equilibration time could be discerned. The exact concentration of denaturant in each sample was determined from its refractive index.  $\Delta G$  values could not be derived because of the deviation from two-state behavior for most of the antibody fragments and, in some cases, the incomplete reversibility due to aggregation.

#### Acknowledgements

This work was supported by the Schweizerische Nationalfonds grant No. 3100-065344/2.

#### References

- Andreaske, E., Taylor, P. C. & Feldmann, M. (2002). Monoclonal antibodies in immune and inflammatory diseases. *Curr. Opin. Biotechnol.* **13**, 615–620.
- Borrebaek, C. A. & Carlsson, R. (2001). Human therapeutic antibodies. *Curr. Opin. Pharmacol.* **1**, 404–408.
- Morino, K., Katsumi, H., Akahori, Y., Iba, Y., Shinohara, M., Ukai, Y. et al. (2001). Antibody fusions with fluorescent proteins: a versatile reagent for profiling protein expression. *J. Immunol. Methods*, **257**, 175–184.
- Siegel, R. W., Allen, B., Pavlik, P., Marks, J. D. & Bradbury, A. (2000). Mass spectral analysis of a protein complex using single-chain antibodies selected on a peptide target: applications to functional genomics. *J. Mol. Biol.* **302**, 285–293.
- Trikha, M., Yan, L. & Nakada, M. T. (2002). Monoclonal antibodies as therapeutics in oncology. *Curr. Opin. Biotechnol.* **13**, 609–614.
- Griffiths, A. D., Williams, S. C., Hartley, O., Tomlinson, I. M., Waterhouse, P., Crosby, W. L. et al. (1994). Isolation of high affinity human antibodies directly from large synthetic repertoires. *EMBO J.* **13**, 3245–3260.
- Knappik, A., Ge, L., Honegger, A., Pack, P., Fischer, M., Wellnhofer, G. et al. (2000). Fully synthetic human combinatorial antibody libraries (HuCAL) based on modular consensus frameworks and CDRs randomized with trinucleotides. *J. Mol. Biol.* **296**, 57–86.
- Nissim, A., Hoogenboom, H. R., Tomlinson, I. M., Flynn, G., Midgley, C., Lane, D. & Winter, G. (1994). Antibody fragments from a "single pot" phage display library as immunochemical reagents. *EMBO J.* **13**, 692–698.
- Nicholson, I. C., Zou, X., Popov, A. V., Cook, G. P., Corps, E. M., Humphries, S. et al. (1999). Antibody repertoire of four- and five-feature translocus mice carrying human immunoglobulin heavy chain and kappa and lambda light chain yeast artificial chromosomes. *J. Immunol.* **163**, 6598–6606.
- Magadan, S., Valladares, M., Suarez, E., Sanjuán, I., Molina, A., Ayling, C. et al. (2002). Production of antigen-specific human monoclonal antibodies: comparison of mice carrying IgH/kappa or IgH/kappa/lambda transloci. *Biotechniques*, **33**, 680 (see also, 682 and 684).
- Batra, S. K., Jain, M., Wittel, U. A., Chauhan, S. C. & Colcher, D. (2002). Pharmacokinetics and biodistribution of genetically engineered antibodies. *Curr. Opin. Biotechnol.* **13**, 603–608.
- Weiner, L. M. & Carter, P. (2003). The rollercoaster ride to anti-cancer antibodies. *Nature Biotechnol.* **21**, 510–511.
- Weir, A. N., Nesbit, A., Chapman, A. P., Popplewell, A. G., Antoniou, P. & Lawson, A. D. (2002). Formattting antibody fragments to mediate specific therapeutic functions. *Biochem. Soc. Trans.* **30**, 512–516.
- Plückthun, A., Krebber, A., Krebber, C., Horn, U., Knüper, U. & Wenderoth, R. (1996). Producing antibodies in *Escherichia coli*: from PCR to fermentation. In *Antibody Engineering* (McCafferty, J., Hoogenboom, H. R. & Chiswell, D. J., eds), pp. 203–252, IRL Press, Oxford.
- Todorovska, A., Roovers, R. C., Dolezal, O., Kortt, A. A., Hoogenboom, H. R. & Hudson, P. J. (2001). Design and application of diabodies, triabodies and tetrabodies for cancer targeting. *J. Immunol. Methods*, **248**, 47–66.
- Plückthun, A. & Pack, P. (1997). New protein engineering approaches to multivalent and bispecific antibody fragments. *Immunotechnology*, **3**, 83–105.
- Vermeer, A. W. & Norde, W. (2000). The thermal stability of immunoglobulin unfolding and aggregation of a multi-domain protein. *Biophys. J.* **78**, 394–404.
- Vermeer, A. W., Norde, W. & van Amerongen, A. (2000). The unfolding/denaturation of immunogammaglobulin of isotype 2B and its Fab and Fc fragments. *Biophys. J.* **79**, 2150–2154.
- Serra, A. & Plückthun, A. (1988). Assembly of a functional immunoglobulin Fv fragment in *Escherichia coli*. *Science*, **240**, 1038–1041.
- Jäger, M. & Plückthun, A. (1999). Folding and assembly of an antibody Fv fragment, a heterodimer stabilized by antigen. *J. Mol. Biol.* **285**, 2005–2019.
- Glockshuber, R., Malia, M., Pfizingher, J. & Plückthun, A. (1990). A comparison of strategies to stabilize immunoglobulin Fv-fragments. *Biochemistry*, **29**, 1362–1367.

22. Hochman, J., Gavish, M., Inbar, D. & Givol, D. (1976). Folding and interaction of subunits at the antibody combining site. *Biochemistry*, **15**, 2706–2710.
23. Horne, C., Klein, M., Polidouli, I. & Dorrrington, K. J. (1982). Noncovalent association of heavy and light chains of human immunoglobulins. III. Specific interactions between  $V_H$  and  $V_L$ . *J. Immunol.* **129**, 660–664.
24. Klein, M., Kortan, C., Kells, D. I. & Dorrrington, K. J. (1979). Equilibrium and kinetic aspects of the interaction of isolated variable and constant domains of light chain with the Fd' fragment of immunoglobulin G. *Biochemistry*, **18**, 1473–1481.
25. Bird, R. E., Hardman, K. D., Jacobson, J. W., Johnson, S., Kaufman, B. M., Lee, S. M. *et al.* (1988). Single-chain antigen-binding proteins. *Science*, **242**, 423–426.
26. Huston, J. S., Levinson, D., Mudgett-Hunter, M., Tai, M. S., Novotny, J., Margolies, M. N. *et al.* (1988). Protein engineering of antibody binding sites: recovery of specific activity in an anti-digoxin single-chain Fv analogue produced in Escherichia coli. *Proc. Natl Acad. Sci. USA*, **85**, 5879–5883.
27. Freund, C., Ross, A., Guth, B., Plückthun, A. & Holak, T. A. (1993). Characterization of the linker peptide of the single-chain Fv fragment of an antibody by NMR. *FEBS Letters*, **320**, 97–100.
28. Shimba, N., Torigoe, H., Takahashi, H., Masuda, K., Shimada, I., Arata, Y. & Sarai, A. (1995). Comparative thermodynamic analyses of the Fv, Fab<sup>+</sup> and Fab fragments of anti-dansyl mouse monoclonal antibody. *FEBS Letters*, **360**, 247–250.
29. Ewert, S., Huber, T., Honegger, A. & Plückthun, A. (2003). Biophysical properties of human antibody variable domains. *J. Mol. Biol.* **325**, 531–553.
30. Ewert, S., Honegger, A. & Plückthun, A. (2003). Structure-based improvement of the biophysical properties of immunoglobulin  $V_H$  domains with a generalizable approach. *Biochemistry*, **42**, 1517–1528.
31. Kaufmann, M., Lindner, P., Honegger, A., Blank, K., Tschopp, M., Capitan, G. *et al.* (2002). Crystal structure of the anti-His tag antibody 3D5 single-chain fragment complexed to its antigen. *J. Mol. Biol.* **318**, 135–147.
32. Jung, S. & Plückthun, A. (1997). Improving in vivo folding and stability of a single-chain Fv antibody fragment by loop grafting. *Protein Eng.* **10**, 959–966.
33. Proba, K., Wörn, A., Honegger, A. & Plückthun, A. (1998). Antibody scFv fragments without disulfide bonds made by molecular evolution. *J. Mol. Biol.* **275**, 245–253.
34. Jermutus, L., Honegger, A., Schwesinger, F., Hanes, J. & Plückthun, A. (2001). Tailoring *in vitro* evolution for protein affinity or stability. *Proc. Natl Acad. Sci. USA*, **98**, 75–80.
35. Rowe, E. S. (1976). Dissociation and denaturation equilibrium and kinetics of a homogeneous human immunoglobulin Fab fragment. *Biochemistry*, **15**, 905–916.
36. Rowe, E. S. & Tanford, C. (1973). Equilibrium and kinetics of the denaturation of a homogeneous human immunoglobulin light chain. *Biochemistry*, **12**, 4822–4827.
37. Wörn, A. & Plückthun, A. (1998). Mutual stabilization of  $V_L$  and  $V_H$  in single-chain antibody fragments, investigated with mutants engineered for stability. *Biochemistry*, **37**, 13120–13127.
38. Liebermann, R., Potter, M., Humphrey, W. J., Mushinsky, E. B. & Vrana, M. (1975). Multiple individual and cross-specific idiotypes of 13 levan-binding myeloma proteins of BALB/c mice. *J. Expt. Med.* **142**, 106–119.
39. Carter, P., Presta, L., Gorman, C. M., Ridgway, J. B., Henner, D., Wong, W. L. *et al.* (1992). Humanization of an anti-p185HER2 antibody for human cancer therapy. *Proc. Natl Acad. Sci. USA*, **89**, 4285–4289.
40. Rudikoff, S. & Pumphrey, J. G. (1986). Functional antibody lacking a variable-region disulfide bridge. *Proc. Natl Acad. Sci. USA*, **83**, 7875–7878.
41. Proba, K., Honegger, A. & Plückthun, A. (1997). A natural antibody missing a cysteine in  $V_H$ : consequences for thermodynamic stability and folding. *J. Mol. Biol.* **265**, 161–172.
42. Kabat, E. A., Wu, T. T., Perry, H. M., Gottesmann, K. S., & Foeller, C. *Sequences of Proteins of Immunological Interest*. NIH Publication no. 1991 91-3242.
43. Schmid, F. X. (1997). Optical spectroscopy to characterize protein conformation and conformational changes. In *Protein Structure—A Practical Approach* (Creighton, T. E., ed.), pp. 261–298. Oxford University Press, Oxford.
44. Myers, J. K., Pace, C. N. & Scholtz, J. M. (1995). Denaturant m values and heat capacity changes: relation to changes in accessible surface areas of protein unfolding. *Protein Sci.* **4**, 2138–2148.
45. Tsunemaga, M., Goto, Y., Kawata, Y. & Hamaguchi, K. (1987). Unfolding and refolding of a type kappa immunoglobulin light chain and its variable and constant fragments. *Biochemistry*, **26**, 6044–6051.
46. Lille, H., Rudolph, R. & Buchner, J. (1995). Association of antibody chains at different stages of folding: prolyl isomerization occurs after formation of quaternary structure. *J. Mol. Biol.* **248**, 190–201.
47. Huston, J. S., Björk, I. & Tanford, C. (1972). Properties of the Fd Fragment from rabbit immunoglobulin G. *Biochemistry*, **11**, 4256–4262.
48. Mhashilkar, A. M., Bagley, J., Chen, S. Y., Szilvay, A. M., Helland, D. G. & Marasco, W. A. (1995). Inhibition of HIV-1 Tat-mediated LTR transactivation and HIV-1 infection by anti-Tat single chain intrabodies. *EMBO J.* **14**, 1542–1551.
49. Cohen, P. A., Mani, J. C. & Lane, D. P. (1998). Characterization of a new intrabody directed against the N-terminal region of human p53. *Oncogene*, **17**, 2445–2456.
50. Tewari, D., Goldstein, S. L., Notkins, A. L. & Zhou, P. (1998). cDNA encoding a single-chain antibody to HIV p17 with cytoplasmic or nuclear retention signals inhibits HIV-1 replication. *J. Immunol.* **161**, 2642–2647.
51. Jäger, M., Gehrig, P. & Plückthun, A. (2001). The scFv fragment of the antibody hu4D5-8: evidence for early premature domain interaction in refolding. *J. Mol. Biol.* **305**, 1111–1129.
52. Eigenbrot, C., Randal, M., Presta, L., Carter, P. & Kossiakoff, A. A. (1993). X-ray structures of the antigen-binding domains from three variants of humanized anti-p185HER2 antibody 4D5 and comparison with molecular modeling. *J. Mol. Biol.* **229**, 969–995.
53. Brandts, J. F., Hu, C. Q., Lin, L. N. & Mos, M. T. (1989). A simple model for proteins with interacting domains. Applications to scanning calorimetry data. *Biochemistry*, **28**, 8588–8596.
54. Ragone, R. (2000). How the protein concentration affects unfolding curves of oligomers. *Biopolymers*, **53**, 221–225.
55. Wörn, A. & Plückthun, A. (1999). Different

- equilibrium stability behavior of scFv fragments: identification, classification, and improvement by protein engineering. *Biochemistry*, **38**, 8739–8750.
56. Wilson, I. A. & Stanfield, R. L. (1994). Antibody-antigen interactions: new structures and new conformational changes. *Curr. Opin. Struct. Biol.* **4**, 857–867.
  57. Prasad, L., Vandonselaar, M., Lee, J. S. & Delbaere, L. T. (1988). Structure determination of a monoclonal Fab fragment specific for histidine-containing protein of the phosphoenolpyruvate: sugar phosphotransferase system of *Escherichia coli*. *J. Biol. Chem.* **263**, 2571–2574.
  58. Rini, J. M., Stanfield, R. L., Stura, E. A., Salinas, P. A., Profy, A. T. & Wilson, I. A. (1993). Crystal structure of a human immunodeficiency virus type 1 neutralizing antibody, 50.1, in complex with its V3 loop peptide antigen. *Proc. Natl Acad. Sci. USA*, **90**, 6325–6329.
  59. Harris, L. J., Larson, S. B., Hasel, K. W. & McPherson, A. (1997). Refined structure of an intact IgG2a monoclonal antibody. *Biochemistry*, **36**, 1581–1597.
  60. Wörn, A. & Plückthun, A. (2001). Stability engineering of antibody single-chain Fv fragments. *J. Mol. Biol.* **305**, 989–1010.
  61. Takahashi, H., Tamura, H., Shimba, N., Shimada, I. & Arata, Y. (1994). Role of the domain-domain interaction in the construction of the antigen combining site. A comparative study by  $^1\text{H}$ - $^{15}\text{N}$  shift correlation NMR spectroscopy of the Fv and Fab fragments of anti-dansyl mouse monoclonal antibody. *J. Mol. Biol.* **243**, 494–503.
  62. Bass, S., Gu, Q. & Christen, A. (1996). Multicopy suppressors of prc mutant *Escherichia coli* include two HtrA (DegP) protease homologs (HtrA/B), DksA, and a truncated RlpA. *J. Bacteriol.* **178**, 1154–1161.
  63. Knappik, A. & Plückthun, A. (1994). An improved affinity tag based on the FLAG peptide for the detection and purification of recombinant antibody fragments. *Biotechniques*, **17**, 754–761.
  64. Gill, S. C. & von Hippel, P. H. (1989). Calculation of protein extinction coefficients from amino acid sequence data. *Anal. Biochem.* **182**, 319–326.

Edited by I. Wilson

(Received 20 October 2004; received in revised form 9 January 2005; accepted 20 January 2005)